A Chemical, Morphological, and Electrochemical (XPS, SEM/EDX, CV, and EIS) Analysis of Electrochemically Modified Electrode Surfaces of Natural Chalcopyrite ($CuFeS_2$) and Pyrite (FeS_2) in Alkaline Solutions

Pablo Velásquez,[†] Dietmar Leinen,[‡] José Pascual,[§] José Ramón Ramos-Barrado,*[,‡] Paula Grez,[||] Humberto Gómez,[||] Ricardo Schrebler,[||] Rodrigo Del Río,[||] and Ricardo Córdova[||]

Instituto de Bioingeniería, Departamento de Ciencia y Tecnología de Materiales, Universidad Miguel Hernández, E03202 Elche (Alicante) Spain, Laboratorio de Materiales & Superficie, (Unidad asociada al CSIC), Departamento de Física Aplicada, Facultad de Ciencias, Universidad de Málaga, E29071 Málaga (Spain), Laboratorio de Materiales & Superficie, (Unidad asociada al CSIC), Departamento de Ingeniería Civil, Materiales y Fabricación, Escuela Técnica Superior de Ingeniería Industrial, Universidad de Málaga, E29071 Málaga (Spain), and Instituto de Química, Facultad de Ciencias Básicas y Matemáticas, Pontificia Universidad Católica de Valparaíso, Casilla 4059, Valparaíso (Chile)

Received: April 21, 2004; In Final Form: November 11, 2004

Electrodic surfaces of natural chalcopyrite and natural pyrite minerals (El Teniente mine, Chile) have been studied by cyclic voltammetry (CV), electrochemical impedance spectroscopy (EIS), X-ray photoelectron spectroscopy (XPS), and scanning electron microscopy including microanalysis (SEM/EDX). For comparison, fractured and polished mineral surfaces were also studied by XPS. In both electrodes, the formation of Fe(III) species containing oxygen were detected and Cu(II) species containing oxygen were additionally detected for chalcopyrite at advanced oxidation states. The presence of Cu(II) species containing oxygen was not detected by XPS for the initial oxidation states of the chalcopyrite. For pyrite, the present results do not allow confirmation of the presence of polysulfurs such as have been previously proposed. In both minerals, the measurements of SEM and EDX show relevant alterations in the respective surfaces when different potential values were applied. The chalcopyrite surface shows the formation of protrusions with a high concentration of oxygen. The pyrite surface shows a layer of modified material with high oxygen content. The modifications detected by XPS, SEM, and EDX allowed the explanation of the complexity of the equivalent circuit used to simulate the experimental EIS data. At high oxidation states, both minerals showed a pseudoinductive loop in the equivalent circuit, which was due to the active electrodissolution of the minerals which takes place through a surface film previously formed.

1. Introduction

In the flotation process of the sulfurous minerals of copper, the surface of the mineral is subject to varying electrochemical processes which considerably alter their physical and chemical properties.[1,2] These processes include redox reactions, adsorption of intermediary elements, superficial interactions, and, in general, diverse electrochemical processes which, in turn, are dependent on the electrode/dissolution interactions. All these processes have a decisive influence on the productivity of the industrial extraction of copper.[3] Electrochemical techniques, especially cyclic voltammetry (CV) and electrochemical impedance spectroscopy (EIS), can be used in the study of these processes and to establish their electrochemical models.[4] They have even been able to distinguish between different processes and, in some cases, to establish their kinetics. However, the assignation of these different processes to specific electrochemical reactions is not free from ambiguity, given that electrochemical methods do not allow for the initial composition of the compounds responsible for these processes to be determined. For this reason, the use of techniques to characterize surfaces such as X-ray photoelectron spectroscopy (XPS) and scanning electron microscopy (SEM) provide a more direct form of establishing the chemical and morphological changes occurring on the surface and hence explaining the electrochemical results obtained. The changes in oxidation states of diverse chemical elements found on the surface of the mineral can be established from XPS, and it is even possible to quantitatively determine the extent of these changes. However, the use of these analytical techniques (XPS, SEM/EDX) require that the electrode surface undergoes no other modifications than those caused by the electrochemical process. These methods require the use of chambers containing a nonoxidizing atmosphere to carry out electrochemical experiments and have them coupled to the spectrometer or microscope in order to allow the electrode to be analyzed without exposing it to the atmosphere. In various previous studies, we have applied this method to the study of other sulfur copper minerals such as enargite and chalcocite.[5−7]

One of the most common sulfur copper minerals found in the mining of copper is chalcopyrite ($CuFeS_2$), and is usually found together with pyrite. Chalcopyrite is a yellow mineral, softer than steel and more brittle than gold;[8,9] it is a semiconductor, and it presents a crystal tetragonal structure ($a = 5.25$ Å; $c = 10.32$ Å) based on zinc blend. Pyrite is also yellow and

* Corresponding author. E-mail: barrado@uma.es.
[†] Universidad Miguel Hernández.
[‡] Facultad de Ciencias, Universidad de Málaga.
[§] Escuela Técnica Superior de Ingeniería Industrial, Universidad de Málaga.
[||] Pontificia Universidad Católica de Valparaíso.

10.1021/jp048273u CCC: $30.25
Published on Web 03/02/2005

is crystallographically isometric ($a = 5.42$ Å); it usually appears in the form of cubic crystals[8,9] like those of NaCl.

The objective of the present work is to apply the analytical CV and EIS electrochemical techniques in conjunction with XPS and SEM/EDX techniques to electrodes of natural chalcopyrite and pyrite in an alkaline Borax solution (pH = 9.2), while they are subject to different potential values which were selected from the corresponding cyclic voltammograms obtained at the same conditions. The main aim is to relate the morphological and chemical changes on the surface of the electrode with changes in the electrochemical parameters as determined by CV and EIS.

2. Experimental Methods

2.1. Cyclic Voltammetry (CV) and Electrochemical Impedance Spectroscopy (EIS). The working electrodes were natural chalcopyrite ($CuFeS_2$) and pyrite (FeS_2), both obtained from the El Teniente company mine (Chile). Their respective crystal structures were determined by XRD. They correspond to chalcopyrite ($CuFeS_2$) (PDF 35-0752) and pyrite (FeS_2) (PDF 6-0710). The sample was placed in epoxy resin. The area of electrode exposed to the electrolyte was 0.2 cm^2. The electrode was attached to the copper wire with eutectic In−Ga. The auxiliary electrode was made of graphite (Goodfellows), and a satured calomel electrode (SCE) (0.242 V vs NHE) from EG&G was employed as the reference electrode. All the potentials mentioned in this work are refereed to this electrode. Before each measurement (i.e., for each applied potential value), a fresh electrode surface was prepared by wet abrading with 600-grade silicon carbide paper and then rinsing with deoxygenated, deionized water. Finally, a fine polish was achieved with an alumina suspension, first with 0.3-μm and later with 0.05-μm particle size.

After each electrochemical treatment, electrode surfaces were cleaned by rinsing with water before XPS or SEM/EDX analysis. The electrolyte solution was prepared with disodium tetraborate decahydrate (Borax) from Merck (EWG-Nr. 215-540-4) to 0.05 M (pH 9.2) in deoxygenated, deionized, and boiled water (DDB water). The constant ionic strength was 0.2. Voltammetry measurements were performed with a computer-controlled electrochemical interface (EI), with Solartron EI 1286 by means of the corresponding software. The Solartron EI 1286 was connected to the electrochemical cell via copper feedthroughs in the glovebox with a diameter of 3 mm. For the chalcopyrite electrode, the potentiodynamic cycles were performed with a positive-going potential sweep (PGPS) from −0.20 V to +0.85 V and back with a negative-going potential sweep (NGPS) from +0.85 V to −0.20 V at a scan rate of 0.005 V s^{-1}. From the potentiodynamic *E*/*I* profile of the chalcopyrite electrode (Figure 1), the potentials chosen for the study of surface modifications in the PGPS were −0.15 V (1), +0.20 V (2), +0.45 V (3), +0.60 V (4), and +0.75 V (5); and in the NGPS were +0.60 V (6), +0.45 V (7), +0.20 V (8), −0.15 V (9), −0. 40 V (10), and −0.60 V (11). Similarly, for the pyrite electrode, the potentiodynamic cycles were performed in PGPS from −0.10 V to +0.65 V and back with an NGPS from +0.65 V to −0.95 V at a scan rate of 0.005 V s^{-1}. From the potentiodynamic *E*/*I* profile of the pyrite electrode (Figure 2), the potentials chosen for the study of surface modifications in the PGPS were +0.10 V (1), +0.40 V (2), and +0.60 V (3); and in the NGPS were +0.60 V (4), +0.40 V (5), +0.10 V (6), −0.20 V (7), −0.50 V (8), and −0.80 V (9).

Once the corresponding potential was attained, the scan was stopped at the electrode potential chosen and maintained for at least 400 s or until a steady-current condition was achieved.

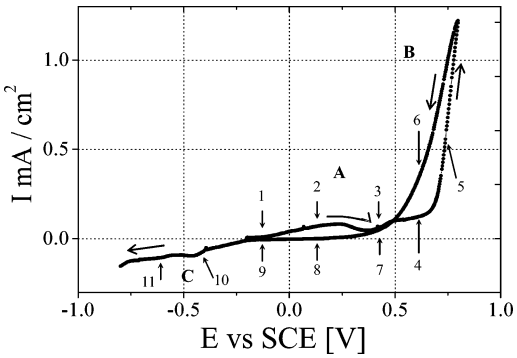

Figure 1. Voltammetry curve *I*/*E* in a borate buffer solution of pH 9.2 for the chalcopyrite. The points of study for surface modifications in the PGPS were −0.15 V (1), +0.20 V (2), +0.45 V (3), +0.60 V (4), and +0.75 V (5); and in the NGPS were +0.60 V (6), + 0.45 V (7), +0.20 V (8), −0.15 V (9), −0.40 V (10), and −0.60 V (11).

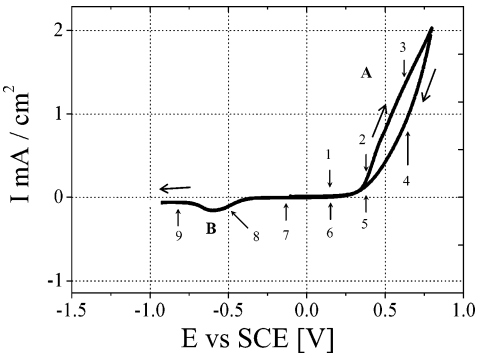

Figure 2. Voltammetry curve *I*/*E* in a borate buffer solution of pH 9.2 for the pyrite. The points of study for surface modifications in the PGPS were +0.10 V (1), +0.40 V (2), and +0.60 V (3); and in the NGPS were +0.60 V (4), +0.40 V (5), +0.10 V (6), −0.20 (7), −0.50 V (8), and −0.80 V (9).

Impedance data were recorded with a Solartron 1255 frequency response analyzer (FRA). For all impedance measurements, the Solartron FRA sine-wave output was superimposed on an applied dc bias from the Solartron EI 1286. The FRA and the EI were both controlled by a computer by means of a specialized program. AC measurements were made for the frequency range from 10 mHz to 10 kHz for different dc applied potentials and an ac potential of 0.01 V rms. Measurements of EIS for both electrodes were carried out at each potential value indicated already. All measurements were performed at 300 K.

2.2. XPS. XPS measurements were performed with a PHI 5700 spectrometer using Mg Kα radiation (1253.6 eV) and Al Kα radiation (1486.6 eV) as excitation sources. Multiregion spectra were recorded at a 45° takeoff angle with a concentric hemispherical energy electron analyzer operating in the constant-pass energy mode at 29.35 eV, using a 720-μm diameter analysis area. Under these conditions, the Au $4f_{7/2}$ line was recorded with 1.16 eV fwhm at a binding energy of 84.0 eV. The spectrometer energy scale was calibrated using Cu $2p_{3/2}$, Ag $3d_{5/2}$, and Au $4f_{7/2}$ photoelectron lines at 932.7, 368.3, and 84.0 eV, respectively. Survey and multiregion spectra were recorded of the Cu 2p, S 2p, Fe 2p, C 1s, O 1s, B 1s, and Na 1s photoelectron peaks. The pressure in the analysis chamber was maintained below ~10^{-7} Pa. A *PHI ACCESS ESCA*, v 6.0F, software package was used for data acquisition and analysis. The atomic concentrations were calculated from the photoelectron peak areas using Shirley background subtraction,[10] and sensitivity factors were provided by the spectrometer manufacturer PHI (Physical Electronics, 6509 Flying Cloud Drive, Eden Prairie, MN 55344, U.S.A.). Recorded spectra were not shifted

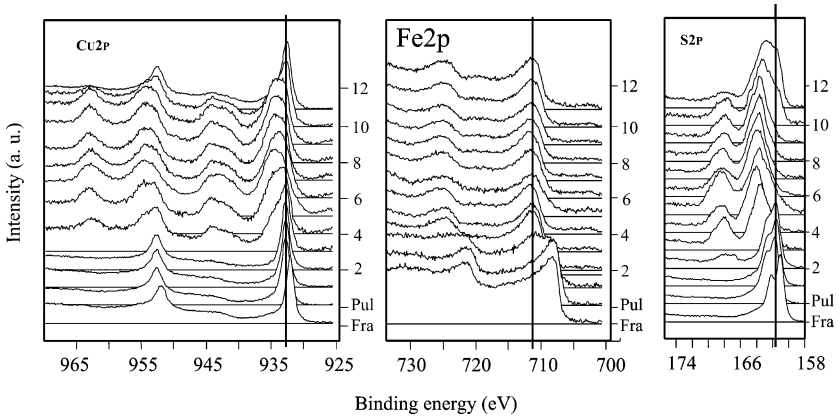

Figure 3. Normalized Cu 2p, S 2p, and Fe 2p XPS spectra recorded after each electrochemical treatment of applied potential for the chalcopyrite electrode surface. The points of study for surface modifications were fractured (Fra) and polished (Pol), and in the PGPS were −0.15 V (1), +0.20 V (2), +0.45 V (3), +0.60 (4), and +0.75 V (5); and in the NGPS were +0.60 V (6), +0.45 V (7), +0.20 V (8), −0.15 V (9), −0.40 V (10), and −0.60 V (11).

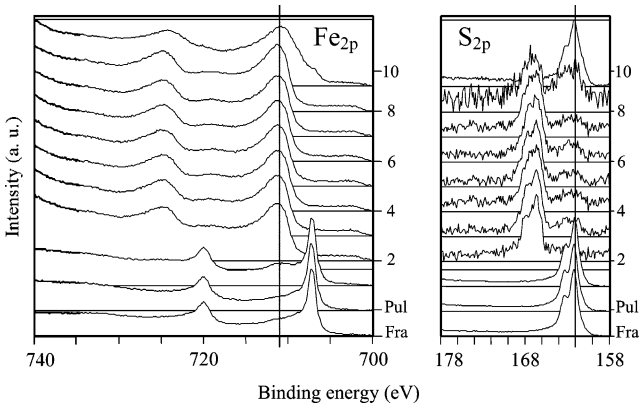

Figure 4. Normalized S 2p and Fe 2p XPS spectra recorded after each electrochemical treatment of applied potential for the pyrite electrode surface. The points of study for surface modifications were fractured (Fra) and polished (Pol), and in the PGPS were +0.10 V (1), +0.40 V (2), and +0.60 V (3); and in the NGPS were +0.60 V (4), +0.40 V (5), +0.10 V (6), −0.20 V (7), −0.50 V (8), and −0.80 V (9).

in binding energy. In fractured chalcopyrite, Cu $2p_{3/2}$ was found at 932.8 eV and, in fractured pyrite, Fe $2p_{3/2}$ at 707.2 eV. After each electrochemical treatment (i.e., for each point of study), the electrode surface was cleaned from residual electrolyte solution by rinsing with DDB water. All this treatment was carried out in the glovebox filled with Ar gas (99.999%) coupled to the spectrometer. Then, Mg Kα and Al Kα survey spectra and multiregion spectra were recorded. In this way, the XPS analyses were carried out for the same points signed in the respective potentiodynamic *E*/*I* profile and EIS experiments without exposure of the electrode surface to ambient atmosphere. For comparison, a fractured mineral surface and a polished mineral surface in the same chamber (Ar atmosphere) was also studied (Figure 3 and Figure 4)

2.3. Scanning Electron Microscopy and EDX. SEM micrographs and EDX spectra were obtained with a JEOL JSM 6400 scanning electron microscope equipped with a Link analytical system. The electron energy used was 20 keV. In this case, the glovebox filled with Ar gas (99.999%) was coupled to the microscope for analysis at each potential value applied. In this way, the SEM and EDX analysis were carried out at the same potential values chosen for the EIS and XPS experiments. After each electrochemical treatment, a cleaning of the electrode surface was carried out with DDB water in the glovebox (filled with Ar) coupled to the SEM/EDX chamber, after which the SEM microphotograph and EDX spectra were recorded.

3. Results and Discussion

3.1. Cyclic Voltammetry. *Chalcopyrite.* Voltammetric experiments had been previously done to determine the contributions of the main currents. These contributions are associated to electrochemical processes occurring on the electrode surface. Figure 1 shows the potentiodynamic *I*/*E* profile in a pH 9.2 borate buffer solution. In the voltammogram, anodic current contributions are observed at +0.30 V (5.32 mC/cm^2) and at +0.70 V (22.13 mC/cm^2), and a cathodic current contribution at −0.4 V (4.82 mC/cm^2), labeled A, B, and C, respectively.

From the potential of −0.3 V onward, it can be considered[11,12] that there is a formation of stable species of $Fe(OH)_3$, Fe_2O_3, and metastable phases of $CuFe_{(1-x)}S_2$ and CuS_2*. The last one represents a limiting composition Cu/2S in which the structure of chalcopyrite is retained. Both species are produced for the migration of iron ions from the chalcopyrite electrode toward the interface electrode/electrolytic solution. Moreover, for potentials more positive than 0.2 V (current contribution A), decomposition of the passivating film of CuS_2* could take place, and $Cu(OH)_2$ and CuO can be formed as products through the following reactions

$$CuS_2^* + 2OH^- \rightarrow Cu(OH)_2 + 2S + 2e^- \quad (1)$$

$$CuS_2^* + 2OH^- \rightarrow CuO + 2S + H_2O + 2e^- \quad (2)$$

For potential values close to +0.7 V (current contribution B), the most probable reactions that take place are[13]

$$2CuFeS_2 + 10OH^- \rightarrow 2CuO + Fe_2O_3 + 4S + 5H_2O + 10e^- \quad (3)$$

$$2CuFeS_2 + 42OH^- \rightarrow Fe_2O_3 + 21H_2O + 4SO_4^{2-} + 34e^- \quad (4)$$

$$2CuFeS_2 + 8OH^- \rightarrow CuFeO_4 + CuS + FeS + 2S + 4H_2O + 8e^- \quad (5)$$

In the preceding reactions, the most remarkable fact is the formation of SO_4^{2-} ions and sulfur. According to reactions 3 and 4, an increase of the local acidity of the electrode interface exists, which in turn, would provoke a partial dissolution of the copper and iron oxides initially formed on the chalcopyrite surface. This phenomenon would be responsible for the

reactivation process, which is observed in the initial part of the NGPS of Figure 1. On the contrary, this reactivation process is not observed when a pyrite electrode is assayed, because the electrooxidation of this mineral species does not provoke a large increase of the interface acidity, and therefore, a major stabilization of the electroformed surface compounds would be taking place. See discussion to follow.

In continuation of the NGPS, the reduction of the remaining compounds formed during the PGPS would take place according to the reactions

$$CuO + S + H_2O + 2e^- \rightarrow CuS + 2OH^- \quad (6)$$

$$2CuO + H_2O + 2e^- \rightarrow Cu_2O + 2OH^- \quad (7)$$

Nevertheless, other reduction processes which are related to the reverse reactions of the oxidation processes (current contribution A) could take place, although with lower probability.

Pyrite. The pyrite voltammogram is very similar to that of chalcopyrite (Figure 2), although somewhat simpler. In fact, in pH 9.2 electrolytic solution, two current contributions are distinguished: the anodic current contribution labeled A (+0.8 V, 100.13 mC/cm^2) and the cathodic current contribution labeled B (−0.55 V, 8.53 mC/cm^2). If the $E-$pH diagram proposed by Tao et al.[14] for the Fe−S−H_2O system is taken into account, the only stable species in the potential range considered here (from −0.95 V to +0.65 V) and in this electrolytic media are $Fe(OH)_3$ and the SO_4^{2-} ion. Therefore, the process associated to the anodic current contribution A would correspond to the following reaction, which has also been proposed by Hamilton and Wood[15]

$$FeS_2 + 11H_2O \rightarrow Fe(OH)_3 + 2SO_4^{2-} + 19H^+ + 15e^- \quad (8)$$

Although these authors also initially proposed the formation of elemental sulfur, lately by means of voltammetric and XPS experiences, they confirmed the existence of a metal-deficient sulfide as the principal sulfur product formed during the electrooxidation of pyrite[16] according to

$$FeS_2 + 3xOH^- \rightarrow xFe(OH)_3 + Fe_{1-x}S_2 + 3xe^- \quad (9)$$

On the other hand, Yoon et al.[17] proposed a process located at a potential close to 0.2 V (that in our experience does not clearly appear in evidence), the formation of polysulfides

$$nFeS_2 + 3(n-2)OH^- \rightarrow 2FeS_n + (n-2)Fe(OH)_3 + 3(n-2)e^- \quad (10)$$

The cathodic current contribution B corresponds to the reduction process of all the species formed in the PGPS. However, the charge of the anodic process A (100.13 mC/cm^2) is much greater than the charge of process B (8.53 mC/cm^2), which indicates that the anodic process taking place is not reversible. The same is found to be true for the chalcopyrite case. In both mineral species, given its own semiconductor character and the semiconductor character of the species formed during its electrooxidation (oxides and hydroxides), p−n connections could be established, hindering the passage of current during the NGPS, although for this occurrence, a homogeneous layer of the compounds would be necessary. A more likely case is that the species formed in oxidation are reduced to produce a cathode crest giving FeS[15] as a reduction product

$$Fe(OH)_3 + S + 3e^- \rightarrow FeS + 3OH^- \quad (11)$$

Nevertheless, reaction 11 has not been considered probable, because the electrode surface, after the NGPS take place, would be converted to one with properties resembling those of pyrrhotite (FeS), which does not occur. In fact, after the electroreduction of the chemical species formed in the PGPS, the electrochemical characteristic of the mineral surface is similar to that of pyrite.[16] Therefore, the current contribution B in the NGPS would be

$$xFe(OH)_3 + Fe_{1-x}S_2 + 3xe^- \rightarrow FeS_2 + 3xOH^- \quad (12)$$

3.2. X-ray Photoelectron Spectroscopy. *Chalcopyrite.* In Table 1, XPS atomic concentrations and atomic ratios of natural chalcopyrite are given. The fractured chalcopyrite mineral surface shows a stoichiometry of $Cu_1Fe_{0.99}S_{1.96}$, which is in good agreement with the bulk composition as determined by XRD (PDF 35-0752). However, the polished electrode surface of the natural mineral reveals an iron-deficient composition, and a large increase in carbon Figure 3 shows the normalized Cu 2p, S 2p, and Fe 2p spectra recorded after each electrochemical treatment of applied potential for 400 s. The spectra of fractured and polished electrode surfaces are include for comparison. The changes in the Cu 2p spectra start from +0.45 V in PGPS onward in the voltammogram, with the widening of the main peaks and the appearance of satellites, which demonstrate the presence of oxidized species on the electrode surface; this state is maintained until to the potential of −0.40 V in NGPS. There are several chemical species that could contribute to these spectra: CuO (933.7 eV), $Cu(OH)_2$ (935.1 eV), $CuSO_4$ (934.9 eV), and $CuFe_2O_4$ (933.7 eV),[18,19] because all the peaks are around 933 eV with fwhms of 4 eV. Moreover, the oxygen region allows all these states of oxidation.

On the other hand, the sulfur region shows large changes after +0.2 V in the PGPS with the appearance of a new peak at about 168 eV, attributable to the presence of SO_4^{2-} (168 eV) and clearly distinguishable from the main peak at 163.7 eV to which, according to the spectra, S^{2-} (161.1 eV), S_2^{2-} (162 eV), and S_n^{2-} (163 eV) would contribute. In the initial spectra, there is a greater influence of S^{2-} (161.1 eV) corresponding to $FeCuS_2$ or to the iron-deficient metastable phases of $CuFe_{1-x}S_2$ or CuS_2*. In spectra 3, 4, and 6−10, its respective contributions decrease notably, and a new signal located at ca. 168 eV would indicate partial recovery of the mineral by newly formed species corresponding to SO_4^{2-} (168 eV). This XPS signal remains unaltered until point 11 where it disappears.

The iron region is characterized by the 2.4 eV displacement of the peak toward higher energy levels from point 1 of the voltammogram that indicates the presence of iron oxides; the absence of its satellites could be due to the formation of different oxide layers that prevent these from being clearly seen. The presence of $Fe_2(SO_4)_3$ (712.3 eV)[13] is possible, given that the peak energy of Fe $2p_{3/2}$ in the spectra of points 2 and 11 is 711.5 eV with an average fwhm of 4 eV. Because this, we propose a new reaction for peak B; moreover, of the corresponding reactions represented by eqs 3−5

$$2CuFeS_2 + 34OH^- \rightarrow CuSO_4 + Fe_2(SO_4)_3 + CuO + 17H_2O + 34e^- \quad (13)$$

TABLE 1: XPS Atomic Concentrations of All Elements and Atomic Ratios of Natural Chalcopyrite

		atomic concentration %					atomic ratio		
spectra	treatment	C	O	S	Fe	Cu	Cu_xFe	$CuFe_x$	CuS_x
fractured	fracture surface	28.49	4.46	33.27	16.71	17.07	1.01	0.99	1.96
polished	polished surface	45.86	9.04	24.71	9.50	10.88	1.15	0.87	2.27
1	−0.15 V in PGPS	51.97	13.43	17.24	8.07	9.28	1.15	0.87	1.86
2	+0.20 V in PGPS	46.32	27.70	8.48	10.02	7.48	0.75	1.34	1.13
3	+0.45 V in PGPS	49.18	34.22	5.06	6.21	5.33	0.86	1.17	0.95
4	+0.60 V in PGPS	42.86	38.06	5.40	6.61	7.07	1.07	0.93	0.76
5	+0.75 V in PGPS	34.64	43.73	4.42	3.01	14.20	4.72	0.21	0.31
6	+0.60 V in NGPS	39.66	38.88	6.21	5.69	9.56	1.68	0.60	0.65
7	+0.45 V in NGPS	38.96	39.63	5.38	6.72	9.31	1.39	0.72	0.58
8	+0.20 V in NGPS	38.20	38.58	5.35	5.74	12.13	2.11	0.47	0.44
9	−0.15 V in NGPS	41.24	36.26	5.27	5.87	10.96	1.87	0.54	0.48
10	−0.40 V in NGPS	38.35	35.82	6.27	7.54	12.02	1.59	0.63	0.52
11	−0.60 V in NGPS	31.71	31.51	11.17	7.83	17.78	2.27	0.44	0.63

Besides, the presence of Fe_2O_3 (710.8 eV), eq 3, and FeOOH (711.8 eV) can be established, and these have been considered as forming a part of the electrooxidation mechanisms of iron in alkaline environments:[20,21]

$$CuFeS_2 + 3OH^- \rightarrow 2CuS_2 + FeOOH + H_2O + 3e^- \quad (14)$$

The elemental sulfur can also be considered as coming from the reaction represented by eq 3, but it is not detected because of the ultrahigh vacuum (UHV) in the XPS chamber. Also, spectra 6−9 of all the regions demonstrate a process of overall oxidation of the surface, because in every region, the spectra remain unchanged, thus demonstrating that they correspond to the same oxidation process, even though the applied potential diminishes.

Copper tends to stay on the surface during the entire oxidation process, the clearest case being that corresponding to +0.75 V in PGPS due to a high concentration of Cu(II). The greatest increases in the proportion of iron ($CuFe_x$ in Table 1) correspond to points 2 and 3 (current contribution A) due to the oxidation state of the iron that facilitates its migration to the electrode/electrolyte interface over the respective migration of copper ion under the electrical field applied.[13] From point 5 onward, iron always maintains a relationship less than one, indicating the formation of surface compounds that contain the different elements. Sulfur decreases in proportion as compared to its initial state. This can be attributed to oxidation of sulfur to sulfur species containing oxygen, which are solubilized during the cleaning step of the electrode, or otherwise a loss of elemental sulfur upon subjecting the sample to a UHV chamber. Nevertheless, during the initial oxidation state of chalcopyrite (−0.15 V PGPS), the copper and sulfur XPS spectra do not change appreciably with respect to the XPS spectra of fractured or polished surfaces of the mineral, indicating that in such conditions an electrochemical process occurs that leads to the electroformation of the metastable phases ($CuFe_{(1-x)}S_2$ and CuS_2*) and Fe(III) species containing oxygen.

Pyrite. The Fe 2p and S 2p XPS spectra of pyrite are shown in Figure 4. For the Fe 2p region, the changes practically start at point 1 (+ 0.1V in PGPS) with the Fe $2p_{3/2}$ peak at 707.2 eV in which a small peak at 711 eV can be seen and which is due to a partial oxidation of the mineral. Iron is at an energy of 711.1 eV in the spectra of the remaining points of the voltammogram, this being very similar to that found for the oxidation states of chalcopyrite and having an average width of 3.3 eV. These oxidation states, as in the case of chalcopyrite, could be due to the presence of iron species containing oxygen such as $Fe(OH)_3$ (710.7 eV)[22,23], but not Fe_2O_3, because this species is not stable in pyrite.[14] Also, the presence of $FeSO_4$ (712.3 eV) is possible.[18,24]

TABLE 2: XPS Atomic Concentrations of All Elements and Atomic Ratios of Natural Pyrite

		atomic concentration %					atomic ratio
spectra	treatment	C	O	S	S′	Fe	Fe_xS_2
fractured	fractured surface	22.03	9.98	44.66	0	23.33	1.03
polished	polished surface	42.98	12.60	32.93	0	11.49	0.70
1	+0.10 V in PGPS	35.26	18.62	31.18	0	14.94	0.96
2	+0.40 V in PGPS	39.42	43.88	0	1.07	15.63	
3	+0.60 V in PGPS	27.95	52.24	0	2.34	17.47	
4	+0.60 V in NGPS	32.41	48.05	0	1.84	17.70	
5	+0.40 V in NGPS	31.57	48.83	0	1.86	17.74	
6	+0.10 V in NGPS	31.27	48.80	0	1.87	18.06	
7	−0.20 V in NGPS	32.41	48.05	0	1.84	17.70	
8	−0.50 V in NGPS	27.94	48.79	0.73	1.46	21.08	
9	−0.80 V in NGPS	25.20	40.06	5.56	0	29.18	10.5

On the other hand, the S 2p peak, at point 1 (0.1 V PGPS) of the voltammogram, does not change with respect to the fractured and polished mineral surfaces and appears at 162.2 eV and corresponds, according to previous results, to pyritic sulfur (S^{2-}).[25]

Therefore, during the initial state of the oxidation of the pyrite surface (+0.1 V PGPS), the most probable reactions that could be taking place are

$$FeS_2 + 3xOH^- \rightarrow xFe(OH)_3 + Fe_{1-x}S_2 + 3xe^- \quad (15)$$

or

$$FeS_2 + 3xOH^- \rightarrow xFeOOH + Fe_{1-x}S_2 + xH_2O + 3xe^- \quad (16)$$

From point 2 onward, the peak of the sulfur species appears at 166.4 eV with a fwhm of 2.3 eV (Table 2), indicating the presence of SO_3^{2-} and SO_4^{2-} in a smaller proportion[26] (168 eV). Furthermore, the peak at 162.2 eV of the pyritic sulfur disappears because the surface of the electrode, unlike chalcopyrite, is completely covered by the compounds formed anodically on peak A of the voltammogram and do not recur until the spectra of points 8 and 9, which correspond to the reduction process of the B peak of the voltammogram where the compounds formed from oxidation are partially eliminated. Another important difference with respect to the spectra for chalcopyrite is that no peaks appear in the polysulfurous energy region (163−164 eV) owing to the reactions represented by eq 10 and proposed by Yoon et al.[17] In fact, the presence of polysulfide species could not be confirmed in the present experimental conditions. The values for the atomic concentra-

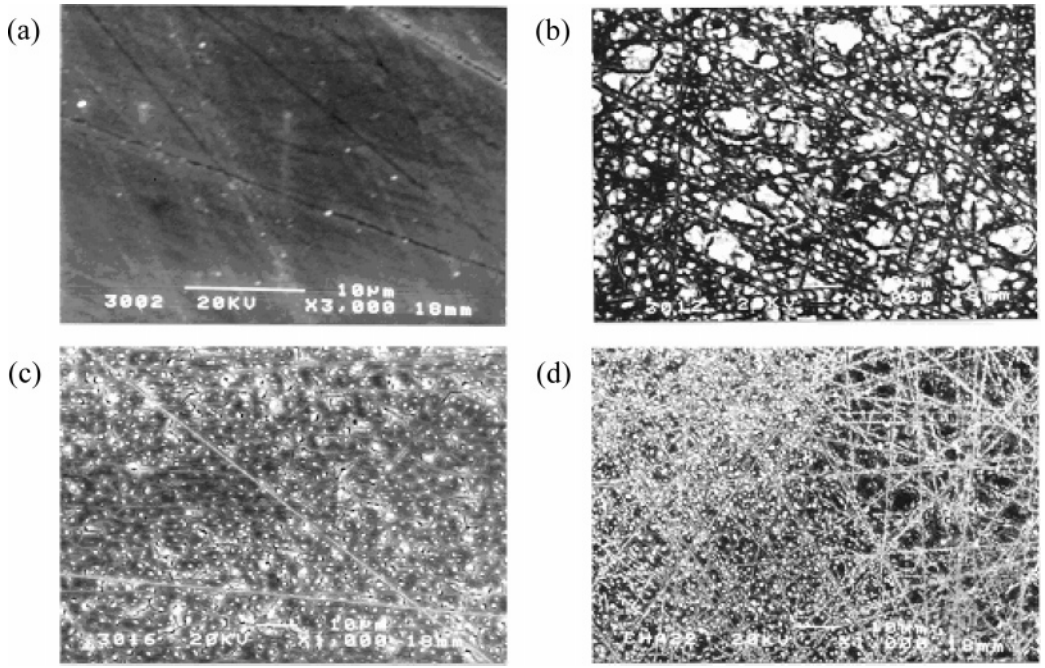

Figure 5. (a) SEM images of the polished electrode surface of chalcopyrite: (b) +0.75 V (PGPS); (c) +0.60 V (NGPS); (d) −0.60 V (NGPS).

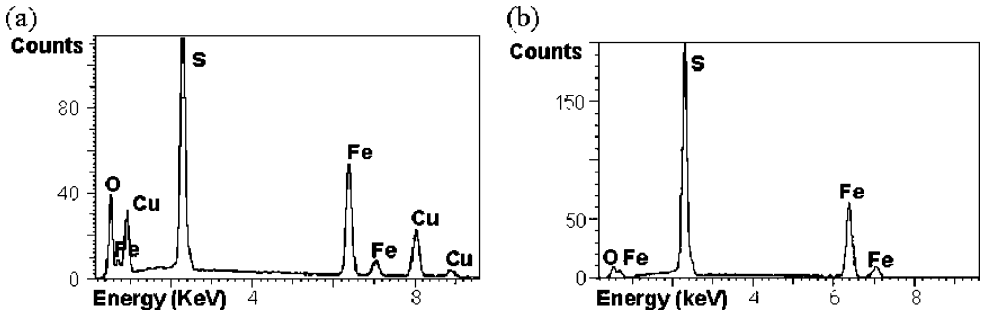

Figure 6. (a) EDX spectra for the protuberance in chalcopyrite at +0.75 V (PGPS), and (b) for the surface layer in the pyrite at +0.60 V (PGPS).

tions of the surface at different potentials are given in Table 2; the calculation for the stoichiometry is made with respect to the peaks for sulfur at 162.2 eV, which corresponds to the surface of the mineral; hence, for the potentials where this peak does not appear, no stoichiometries were calculated.

Therefore, for advanced states of electroxidation of pyrite (in the potential range of 0.4 V to 0.6 V of the PGPS), the following electrochemical reactions on the electrode surface would take place:

$$FeS_2 + 16OH^- \rightarrow FeSO_4 + SO_4^{2-} + 8H_2O + 14e^- \quad (17)$$

$$FeS_2 + 19OH^- \rightarrow FeOOH + 2SO_4^{2-} + 9H_2O + 15e^- \quad (18)$$

$$FeS_2 + 19OH^- \rightarrow Fe(OH)_3 + 2SO_4^{2-} + 8H_2O + 15e^- \quad (19)$$

On the other hand, when the potential applied to the electrode was −0.8 V in the NGPS (point 9), the respective XPS spectra of S 2p and Fe 2p show signals corresponding to pyritic sulfur (162.2 eV) and pyritic iron (707 eV). The last one appears smaller than the signal corresponding to the iron species containing oxygen (711.1 eV). This fact is indicative that, at this potential value, the pyrite surface is partially reestablished through the reverse reactions 15 and 16.

3.3. SEM/EDX. *Chalcopyrite.* The surface of the polished electrode shows a striated, flat surface with small cracks and holes. (Figure 5a). Analysis with EDX of the surface shows a composition, taking into account the range of error, similar to the stoichiometry of chalcopyrite, because $CuFeS_{1.9}$ is obtained. This is in agreement with XPS results for fractured chalcopyrite. The results obtained by SEM and EDX for different points in the PGPS show no variation either in morphology or chemical composition, except for the measurement done at the potential of +0.75 V, where the presence of protuberances unequally distributed and with varying size and brightness can be seen (Figure 5b). This potential value corresponds to the highest anodic current value in the voltammogram (Figure 1), where a mixture of different Cu(II) and Fe(III) oxygen-containing species are formed. According to the XPS data in Table 1, the oxidation of the electrode surface at this potential value is partial; results are in accordance with the EDX data obtained from the diagram shown in Figure 6a. These results allow us to affirm that the electrode surface is composed of a very superficial heterogeneous layer of oxidized materials from which protrude islands formed by grains of oxide, hydroxide, and sulfate materials. The partial reduction process of the surface is observed when the potential moves in the NGPS and is appreciated in the SEM image of the electrode at +0.60 V and −0.60 V, both in NGPS (Figure 5c,d). In fact, a decrease in the sizes of the protuberances is observed, and they have a very similar chemical composition to those protuberances shown in Figure 5b, although with a slight decrease in the quantity of oxygen.

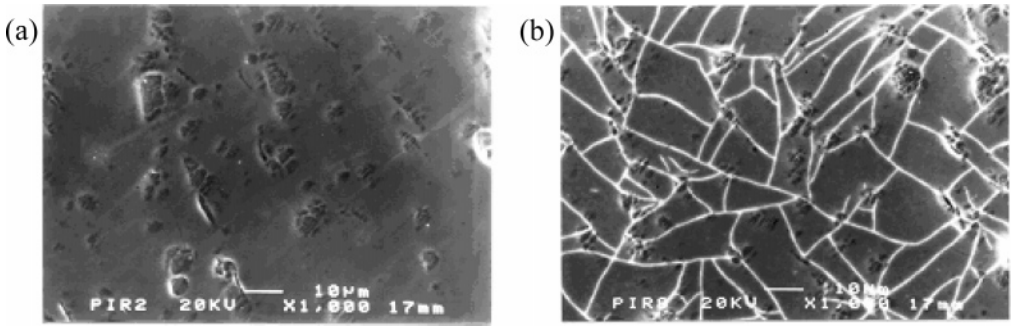

Figure 7. SEM images of (a) polished electrode surface of pyrite and (b) pyrite electrode polarized at +0.60 V (PGPS).

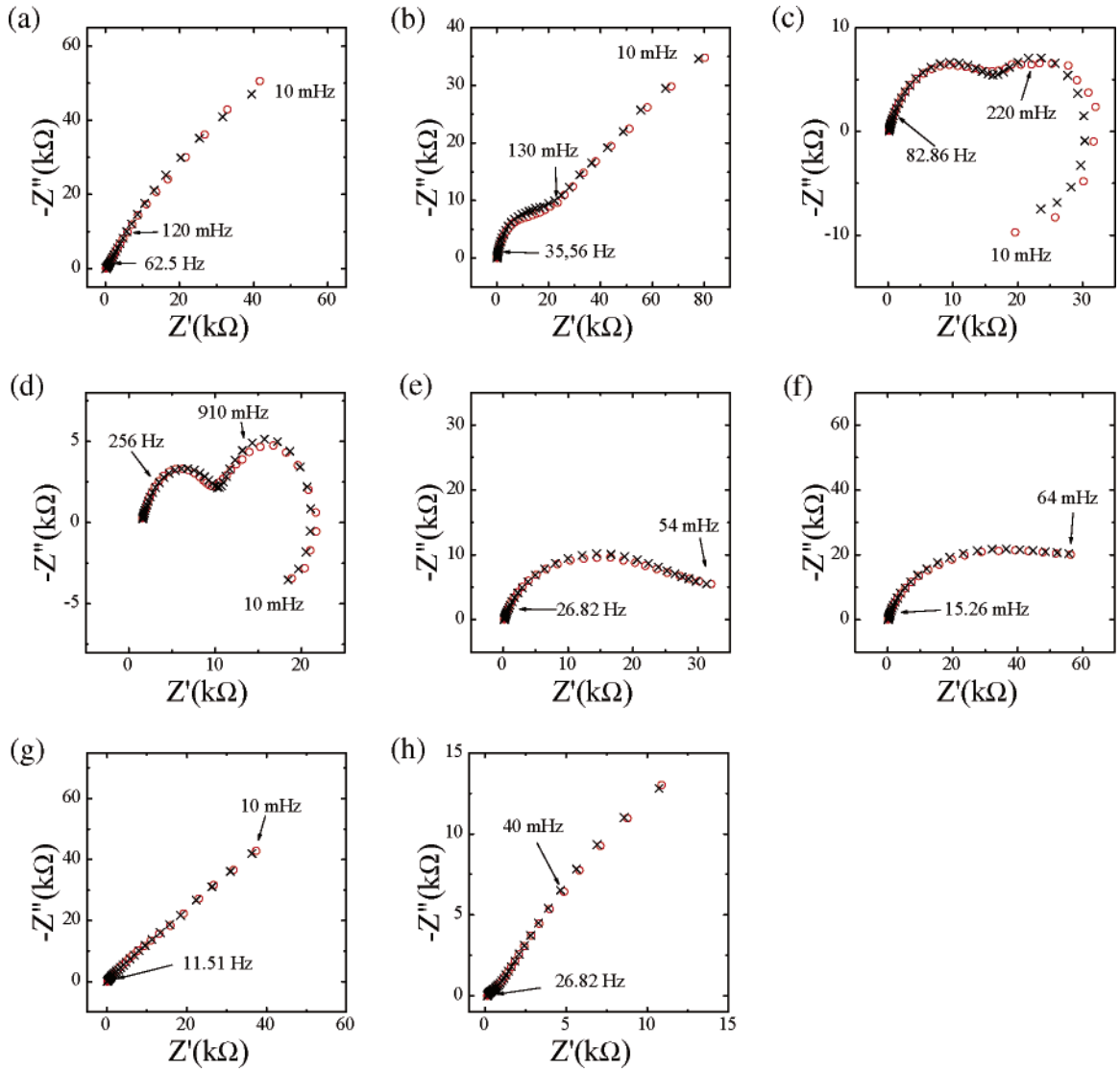

Figure 8. Nyquist plots for the chalcopyrite in the PGPS: $V_{dc} = -0.15$ V (a), +0.20 V (b), +0.45 V (c), and +0.60 V (d), and in the NGPS: $V_{dc} = +0.30$ (e), +0.20 V (f), −0.15 V (g), and −0.40 V (h); where (○) experimental and (×) simulated.

Pyrite. The SEM image of the fractured material (Figure 7a) shows a rough surface with protuberances of the mineral itself. The EDX spectra show a very similar chemical composition to that obtained from XPS. The main modification of the surface of the electrode occurs at +0.60 V in PGPS. At this potential, in Figure 7b, the presence of a modified layer which totally covers the surface is observed which appears cracked by the drying in the UHV chamber. It should be emphasized that the resultant material is virtually transparent to SEM and only can be seen by virtue of its cracks. The EDX spectra (Figure 6B) demonstrate the presence of oxygen, although to a lesser extent than expected, because the EDX spectra are highly influenced by the material underlying the first layers of oxidized material. For the potential values corresponding to NGPS, the material surface is not different from that fractured material because of a decrease in thickness of the layer of modified material which is not cracked, and it cannot be observed by SEM (not shown). However, the EDX spectra show the presence of oxygen, albeit to a lesser extent than observed for the potentials in PGPS.

3.4. Electrochemical Impedance Spectroscopy. *Chalcopyrite*. In CV measurements, values of dc voltage were applied to a natural chalcopyrite mineral electrode from −0.2 V to

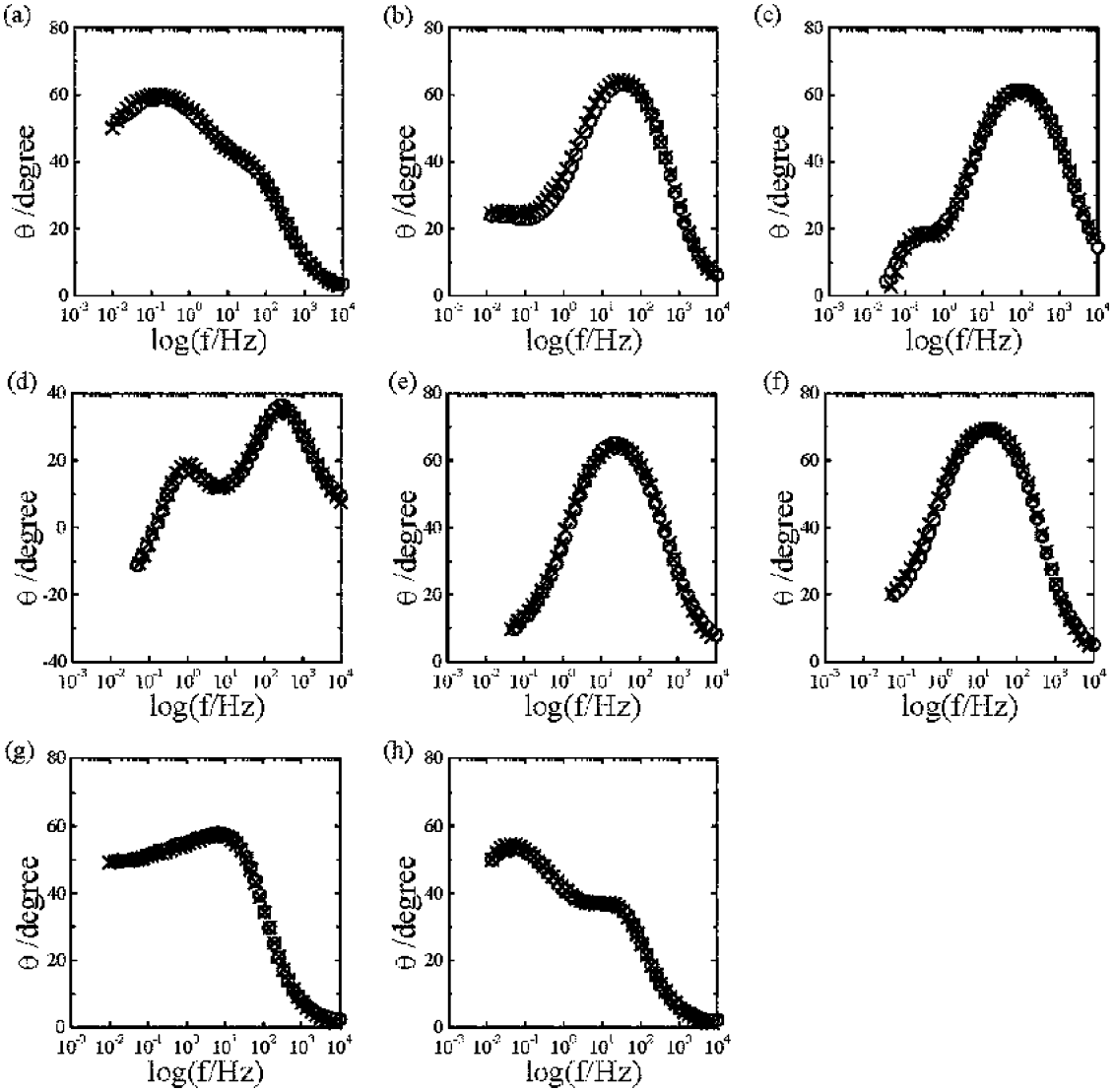

Figure 9. Bode plots for the chalcopyrite in the PGPS: $V_{dc} = -0.15$ V (a), $+0.20$ V (b), $+0.45$ V (c), and $+0.60$ V (d), and in the NGPS: $V_{dc} = +0.30$ (e), $+0.20$ V (f), -0.15 V (g), and -0.40 V(h); where (○) experimental and (×) simulated.

$+0.85$ V PGPS, then to -0.20 V NGPS. All EIS measurements were done with a clean electrode, starting from -0.20 V, then cycling at a scan rate of 0.005 V s^{-1} to the measured potential. Once the working potential was attained, it was maintained for 400 s or until a steady-state current was observed, then the EIS measurements were performed. Data were fitted to equivalent electrochemical circuits by a nonlinear method.[27] The equivalent circuits represent an approach to the description of the electrochemical processes that take place in the electrode/electrolyte interface, and any models derived from them are only tentative.[28]

The EIS measurements were taken at the same potential values as for SEM and EDX measurements. Figure 8 and Figure 9 show the Nyquist and Bode plots for the phase angle, respectively. Figure 10 shows the equivalent circuits employed to fit the experimental data. The values of the different elements in the equivalent circuit are shown in Table 3; to facilitate the interpretation of results, we are including a column with the calculated values of the pseudocapacitance, if it possible to calculate it from the expression $C_{ps} = (Y_0R)^{1/n}R^{-1}$ where $Y_0 = {}^1/_Q$; this expression is valid only for a parallel association of a resistor and a constant-phase element (CPE).

The circuit for the potential of -0.150 V in PGPS corresponds to three relaxation processes (Figure 10a): R_e is the resistance of the electrolyte and other ohmic resistances; R_{ct} is the charge

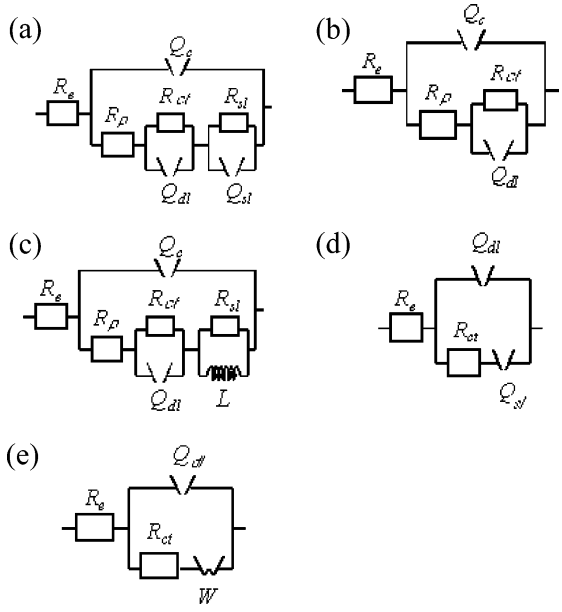

Figure 10. Equivalent circuits: (a) three relaxation processes; (b) two faradaic processes; (c) pseudoinductive loop; (d) modified Randle's; (e) Randle's circuit.

TABLE 3: Values of Elements of the Equivalent Circuits for Different Potentials Applied along the Voltammogram of Chalcopyrite

treatment	$10^4\,Q_c$ ($\Omega\cdot s^{-n}$)	n	R_p (Ω cm^2)	R_{ct} (Ω cm^2)	$10^4\,Q_{dl}$ ($\Omega.s^{-n}$)	n	$10^4\,C_{dl}$ (F cm^{-2})	R_{sl} (Ω cm^2)	$10^4\,Q_{sl}$ ($\Omega.s^{-n}$)	n	$10^4\,C_{sl}$ (F cm^{-2})	L (H)
−0.15 V in PGPS	0.4157	0.76	204.2	11986	0.7376	0.66	10.27082	17434	2.377	0.97	2.16855	
+0.20 V in PGPS	0.08361	0.8	3294	7854	0.6662	0.73	10.28117					
+0.45 V in PGPS	0.04483	0.7	26.46	3092	0.9346	0.95	5.63146	3750				0.2607
+0.60 V in PGPS	0.09567	0.7	25.12	2368	0.2417	0.96	21.54875	19570				0.2767
+0.45 V in NGPS				4294	0.07728	0.81	79.87629		1.237	0.22		
+0.20 V in NGPS				5224	0.06835	0.85	86.06222		0.3224	0.21		
−0.15 V in NGPS				423	0.3222	0.84	18.47418		0.6657	0.49		
−0.40 V in NGPS	0.5332	0.81	115.02	2480	4.398	0.47	2.41889	7536	5.333	0.86	1.09018	

transfer resistance; Q_c corresponds to the capacitance of a coating layer, which is initially present and is formed spontaneously during the polishing of the electrode. This coating layer would correspond mainly to a phase of $CuFe_{1-x}S_2$ and iron species containing oxygen. R_p is the pore resistance of this film, Q_{dl} is the double-layer capacitance, and $R_{sl}-Q_{sl}$ refer to the adsorption species such as iron species. Q_c, Q_{sl}, and Q_{dl} were modeled by a CPE.[28] The CPE is a distributed element defined as $Q = 1/Kp^n$, $0 \le n \le 1$. In this expression, n is a dimensionless number, K is a constant whose dimension is F s^{n-1} cm^{-2}, and $p = j\omega$ with $\omega = 2\pi f$. Q is equivalent to the impedance having a capacitance of $C = K(2pf)^{n-1}$. Therefore, the CPE behaves as a capacitance which varies with the frequency. This modification to an ideal capacitance has already been explained by distribution effects,[29] porosity,[30] fractal geometry,[31] or more recently, by the distribution of interfacial capacitances.[32,33]

For the potential of +0.20 V in PGPS, the equivalent circuit is shown in Figure 10b. This circuit corresponds to two faradaic relaxation processes. This potential is located on the current contribution labeled A in Figure 1. At this potential, intermediary species of Fe(III) are formed which increase the amount of FeOOH and/or Fe_2O_3 in the film. This is in agreement with the XPS results. The change in the equivalent circuit is accompanied by a decrease of Q_c and R_{ct} values together with an important increase in the R_p value, indicating that the kinetics of the electrochemical process and the thickness and porosity of the film on the electrode surface ($CuFe_{1-x}S_2$ and oxohydroxo species of iron) are increased. For potentials of +0.45 and +0.60 V in PGPS, considerable changes can be observed in the Nyquist and Bode plots, showing two loops: one at high frequency which shows a capacitive loop, while the one at low frequencies corresponds to a pseudoinductive loop. The equivalent circuit for both potentials, Figure 10c, is composed of two subcircuits: one formed from the association parallel to a CPE, with Q_{dl} and R_{ct} representing the double-layer capacitance and the resistance of the electron transfer of the electrochemical process, and the other one is formed by R_{sl}, which corresponds to the resistance associated to the accumulation of superficial species, and an inductive element L. This element L may be due to the transfer of ions across the double layer or an increase of the area of the electrode by the partial dissolution of the surface film.[34] The values obtained are given in Table 3, emphasising the change in the values of R_{sl}, which change from 18.75 kΩ to 97.85 kΩ. If we consider the electrochemical reactions associated to the current contribution B (equation 4) and the atomic ratio shown in Table 1, the sulfur ions should be diffusing across the interfaces for their oxidation to sulfate ions. Meanwhile, Cu(II) and Fe(III) ions are also generated and precipitated as CuO and Fe_2O_3 by means of a mechanism of dissolution−precipitation. In this potential range, R_{ct} decreases, owing to

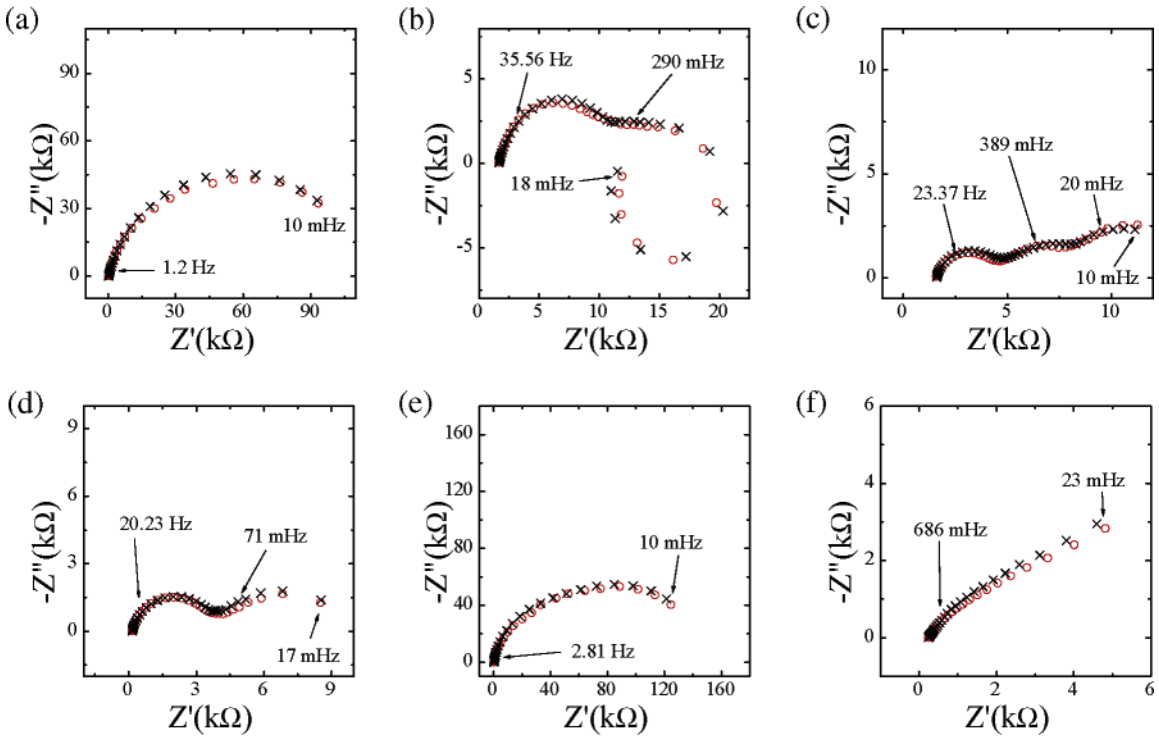

Figure 11. Nyquist plots for pyrite: (a) V_{dc} = +0.10 V (PGPS); (b) V_{dc} = +0.40 V (PGPS); (c) V_{dc} = +0.60 V (PGPS); (d) V_{dc} = +0.30 V (NGPS); (e) V_{dc} = +0.10 V (NGPS); (f) V_{dc} = −0.50 V (NGPS). Experimental data (○) and simulated data (×).

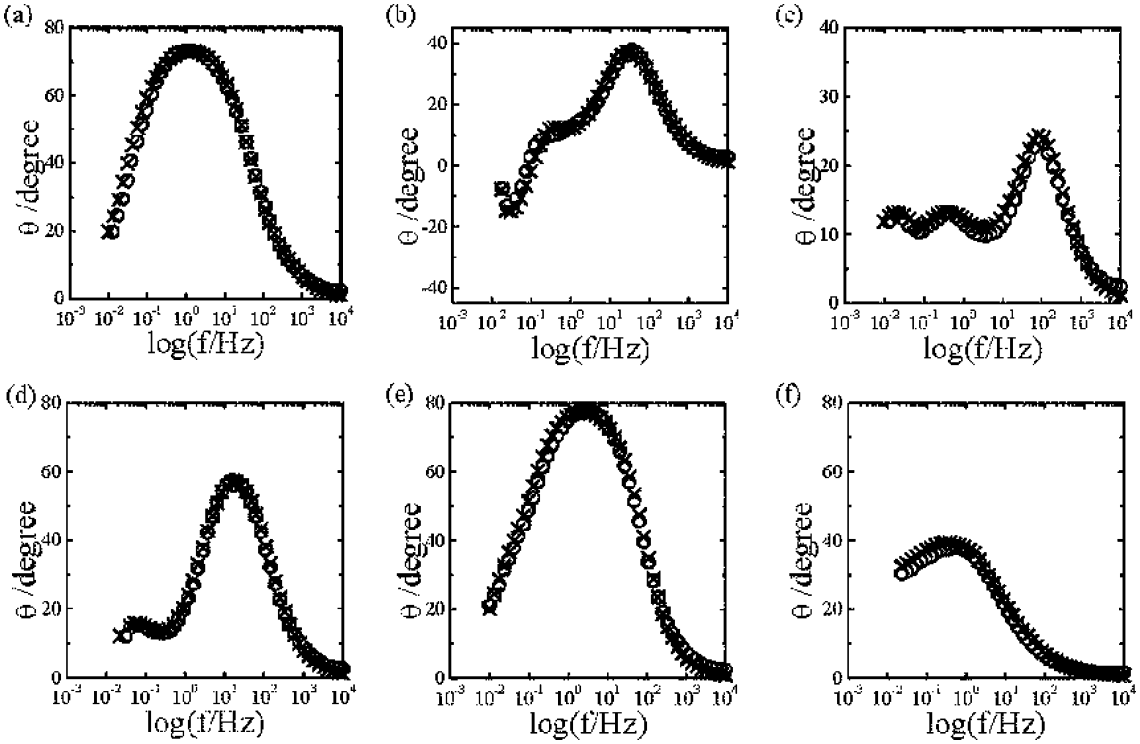

Figure 12. Bode plots for pyrite: (a) $V_{dc} = +0.10$ V (PGPS); (b) $V_{dc} = +0.40$ V (PGPS); (c) $V_{dc} = +0.60$ V (PGPS); (d) $V_{dc} = +0.30$ V (NGPS); (e) $V_{dc} = +0.10$ V (NGPS); (f) $V_{dc} = -0.50$ V (NGPS). Experimental data (○) and simulated data (×).

TABLE 4: Values of Elements of the Equivalent Circuits for Different Potentials Applied along the Voltammogram of Pyrite

treatment	$10^4\ Q_c$ ($\Omega \cdot s^{-n}$)	n	R_p (Ω cm^2)	R_{ct} (Ω cm^2)	$10^4\ Q_{dl}$ ($\Omega \cdot s^{-n}$)	n	$10^4\ C_{dl}$ (F cm^{-2})	R_{sl} (KΩ)	L (H)
+0.10 V in PGPS	0.1255	0.90	22.42	22880	0.2264	0.88	25.09637		
+0.40 V in PGPS	0.3715	0.81	0.026	1631.4	9.621	0.98	0.5303	1.039	0.3394
+0.60 V in PGPS	0.2186	0.87	0.032	269	17.71	0.58	0.48677	0.3093	0.07848
+0.40 V in NGPS	0.2269	0.86	758.8	565	12.80	0.93	0.42003		
+0.10 V in NGPS	0.2199	0.91	19620	9692	1.429	0.98	3.57036		
−0.50 V in NGPS	0.1077	0.92	2.342	2722	4.904	0.59	1.72809		

the increase of the potential and the active dissolution that is conducive to the formation of a superficial floppy film.

The circuit corresponding to +0.30 V and +0.20 V in the NGPS is of a modified Randles type (Figure 10d), which contains a CPE. This circuit describes the response of a single-step charge transfer process.[35] In this circuit, R_{ct} is associated with the charge transfer resistance of the reduction step, which can be represented by eqs 6 and 7.[20] Moreover, the n value of the Q_{sl} element is very small, and now, this element better represents a resistor due to the formation of a layer of CuS, which is more resistive than CuO. For the potential of −0.15 V in NGPS, the equivalent circuit is now a typical Randles circuit (Figure 10e). The Warburg impedance, W, is associated to the diffusion of the OH^- ions produced by the reactions discussed already. For the last applied potential, −0.40 V in NGPS, the equivalent circuit corresponds to three relaxation processes, as does the circuit for the third point (−0.15 V in PGPS). Q_{dl} increases from 0.74 to 4.4 because of an increase of the ionic adsorption in the products of the electrode surface. At this potential, according to the XPS data (Figure 3 and Table 1) the reactions that are taking place would be those that allow a partial regeneration of the chalcopyrite phase[13] (peak E, reactions 1, 2, and 3 in ref 12), which remains a complex film of iron species containing oxygen. These electrochemical reactions promote an important amount of OH^- ions, which can be principally adsorbed by the iron oxides and are therefore responsible for the increase in the Q_{dl} value observed at this potential.

Pyrite. In general, the electrical circuits used for the pyrite system are fewer than those used for chalcopyrite. Figures 11 and 12 show the Nyquist plot and the Bode plot, respectively, and the equivalent circuits employed are some of the ones shown in Figure 10. Only two types of equivalent circuit were necessary for the measurements realized at the potentials chosen from the PGPS of the voltammogram. The first corresponds to a circuit with two relaxation processes (Figure 10b) through the adsorption of an intermediate chemical species, and the second includes a pseudoinductive loop (Figure 10c). Both circuits have been previously discussed for chalcopyrite. For the potential of +0.10 V in PGPS, like that for the chalcopyrite, the equivalent circuit could correspond to the release of iron ions from the mineral structure by means of a dissolution−precipitation mechanism that would give rise to FeOOH or $Fe(OH)_3$ species according to reactions 15 and 16. For the potentials of +0.2 V and +0.4 V in PGSP, the pseudoinductive subcircuit incorporated could be related to the transfer of SO_4^{2-} ions across the double layer, leaving a mineral surface prone to active electrodissolution through reactions 17−19. The most important results are shown in Table 4, emphasizing the strong decrease in the transfer resistance R_{ct}, which changes from 114.4 kΩ (−0.1 V PGPS) to 1.3 kΩ (+0.6 V PGPS), which supposes an important increase in the rate of the electrochemical process that takes place on the mineral surface at these potentials. Moreover, the value of parameter L in the electrical circuit corresponding to the potential of +0.6 V is decreased by four times with respect to the value obtained at +0.4 V, because of greater coverage of

the electrode for the iron species containing oxygen. Nevertheless, the superficial film has low porosity in both potential values, showing a floppy nature of this film, which has no effect on the kinetics of the electrodissolution of the pyrite.

For the potentials measured in the NGPS of the voltammogram, a single equivalent circuit is required which contains two relaxation processes (Figure 10b) and which was used to represent the adsorption species formed in great quantities in the PGPS.

The most important difference can be observed in the R_p values. In fact, at the potential of 0.4 V, where an electrooxidation process is yet taking place, the R_p value is 3.8 kΩ, which is remarkably greater than the value obtained at the same potential value in PGPS. This difference can be explained by considering that, at this potential in the NGPS, the electrode surface is not clean and appears, to a great extent, to be covered by Fe(III) species containing oxygen which suffer from a process of aging, producing a more porous film. The R_{ct} values do not change remarkably. At the potential of +0.1 V in the NGPS, the R_p value increased with respect to the corresponding value in the PGPS, because of the different nature of the surface films that are present in both potential values. Again, R_{ct} values do not show important differences in both experimental conditions. When the potential is changed to −0.5 V in the NGPS, the R_p value is decreased significantly. At this potential, a complex electroreduction process is taking place that considers the reduction of Fe(III) species containing oxygen to $Fe(OH)_2$ and the electroreduction process that corresponds to the reverse of reaction 16, which leads to a partial regeneration of the pyrite surface.[16]

4. Conclusions

The application of surface analysis techniques together with electrochemical techniques allows the relationship between the morphological and chemical changes on the electrode surface. Changes determined by XPS and SEM/EDX were related to the changes in the electrochemical parameters obtained from EIS at different potentials along the potentiodynamic profile *I*/*E* of chalcopyrite and pyrite in a pH 9.2 electrolytic solution. It allowed us to reject or to confirm the electrochemical reactions that take place at the different potentials studied. In the case of chalcopyrite, the presence of Cu(II) is not detected in XPS for potentials lower than 0.30 V in PGPS, but Fe(III) species containing oxygen are always present Therefore, in the initial state of the electrooxidation of chalcopyrite ($E \leq 0.3$ V) an iron-deficient chalcopyrite phase is formed. At more positive potentials, XPS data show the presence of Cu(II), Fe(III), and sulfur species containing oxygen according to reaction 4. Nevertheless, reactions 1−3 could be occurring too, but elemental sulfur could not be detected, because of a possible evaporation of this element under the experimental conditions assayed in the XPS experience. In the case of pyrite, the XPS data for sulfur allow us to discard the presence of polysulfides in the present experimental conditions. Therefore, reaction 10, proposed by Yoon et al.,[15] could not be endorsed.

In the electrochemical modification process of the surfaces of these minerals, significant differences are found. In the case of chalcopyrite, the modified material in the anodic processes forms islands that partially cover the electrode surface. However, in the case of pyrite, the modified material completely covers the electrode surface. These different degrees of cover could be due to different oxidation processes or a partial dissolution of the compounds formed on the surface of the chalcopyrite electrode. For both minerals, Fe(III) species containing oxygen are formed ($Fe(OH)_3$, FeOOH, etc.) with the exception of Fe_2O_3, which is only found in chalcopyrite, the greatest difference being in the copper compounds The difference in the cover of the electrodes and in the mechanisms for the modification of the surface are reflected in the number of equivalent circuits necessary to describe the electrochemical processes in the EIS study. The major complexity found for chalcopyrite in the PGPS is due to the presence of a more complex surface film than for pyrite. Nevertheless, both mineral surfaces show pseudoinductive loops at the potential values close to the respective maximum current contributions, because of the active electrodissolution of the mineral through the surface film previously formed. In both minerals, the oxidation processes were irreversible, because the charge accumulated in the anodic current contribution of the voltammograms is greater than that corresponding to the cathodic current contribution. Therefore, in the NGPS of the voltammogram, only a partial reduction of the products obtained in the PGPS was attained.

Acknowledgment. The financial support of the Junta de Andalucia (Spain) through research group FQM192 and FONDECYT (Chile) through contract 8000022 is gratefully acknowledged.

References and Notes

(1) Buswell, A. M.; Nical, M. J. *J. Appl. Electrochem.* **2002**, *32*, 1321.
(2) Kantar, C. *Colloid Surf., A* **2002**, *210*, 23.
(3) Klimpel, R. R. *Int. J. Miner. Process.* **2000**, *58*, 77.
(4) Cordova, R.; Gomez, H.; Real, S. G.; Schrebler, R.; Vilche, J. R. *J. Electrochem. Soc.* **1997**, *44*, 2628.
(5) Velasquez, P.; Leinen, D.; Pascual, J.; Ramos-Barrado, J. R.; Cordova, R.; Gómez, H.; Schrebler, R. *J. Electroanal. Chem.* **2000**, *494*, 87.
(6) Velasquez, P.; Pascual, J.; Ramos-Barrado, J. R.; Cordova, R.; Leinen, D. *Surf. Interface Anal.* **2000**, *30*, 149.
(7) Velasquez, P.; Leinen, D.; Pascual, J.; Ramos-Barrado, J. R.; Cordova, R.; Gomez, H.; Schrebler, R. *J. Electroanal. Chem.* **2001**, *510*, 20.
(8) *Dictionary of Inorganic Compound*; Macintyre, J. E., Ed.; Chapman and Hall: London, 1992; pp 3100 and 3281.
(9) Wells, A. F. *Structural Inorganic Chemistry*; Oxford University Press: New York, 1967; pp 531 and 520.
(10) Shirley, D. S. *Phys. Rev. B* **1972**, *5*, 4709.
(11) Pourbaix, M. *Atlas of Electrochemical Equilibrium in Aqueous Solutions*; National Association of Corrosion Engineers: Houston, 1974.
(12) Kelsall, G. H.; England, K. E. R.; Vaughan, D. J.; Yin, Q. *Proc. Int. Symp. Electrochem. Miner. Met. Process. III, 3rd, 1992* **1992**, *92*, 318.
(13) Yin, Q.; Vaughan, D. J.; England, K. E. R.; Kelsall, G. H.; Brandon, N. P. *J. Electrochem. Soc.* **2000**, *147*, 2945.
(14) Tao, D. P.; Li, Q.; Richardson, P. E.; Yoon, R. H. *Colloid Surf., A* **1994**, *93*, 229.
(15) Hamilton, I. C.; Woods, R. *J. Electroanal. Chem.* **1981**, *118*, 327.
(16) Buckley, A. N.; Hamiltong, I. C.; Woods, R. In *Proceedings of the International Symposium on Electrochemistry in Mineral and Metal Processing 2*; Richardson, P. E., Wood, R., Eds.; The Electrochemical Society: Pennington, NJ, 1988; pp 234−246.
(17) Yoon, R. H.; Lagno, M. L.; Latrell, G. H.; Mielczark, A. In *Processing and Utilization of High Sulfur Coals IV*; Dugau, P. R., Quigley, D. R., Attia, Y. A., Eds.; Elsevier: Amsterdam, 1991; p 291.
(18) Mcintyre, N. S.; Cook, M. G. *Anal. Chem.* **1975**, *47*, 2208.
(19) Siriwardene, R. V.; Cook, J. M. *J. Colloids Interface Sci.* **1985**, *108*, 414.
(20) Schrebler, R.; Guzmán, J.; Vilche, J. R.; Arvia, J. *Electrochim. Acta* **1979**, *24*, 395.
(21) Gomez, H.; Schrebler, R.; Cordova, R.; Casanova, J.; Velasquez, P. *Bol. Soc. Chil. Quim.* **1997**, *42*, 207.
(22) Donato, P. H.; Mustin, C.; Beboit, R.; Erre, R. *Appl. Surf Sci.* **1993**, *68*, 147.
(23) Mcintyre, N. S.; Zetaruk, D. G. *Anal. Chem.* **1977**, *49*, 1521.
(24) Bonnissel-Gissinger, P.; Almot, M.; Ehrhardt, J. J.; Behra, P. *Environ. Sci. Technol.* **1998**, *32*, 2839.
(25) Nakai, I.; Sugitami, Y.; Nagashima, K.; Niwa, Y. *J. Inorg. Nucl. Chem.* **1978**, *40*, 789.
(26) Nesbiltt, H. W.; Muir, I. J.; Pratt, A. R. *Geochim. Cosmochim. Acta* **1995**, *59*, 1773.

(27) Boukamp, B. A. *Solid State Ionics* **1986**, *26*, 31.
(28) Macdonald, J. R. *J. Appl. Phys.* **1985**, *58*, 1971.
(29) Brug, G. J.; Van den Eden, A. L. G.; Sluyters-Rehbach, M.; Sluyters, H. J. *J. Electroanal. Chem.* **1984**, *176*, 275.
(30) Gassa, L. M.; Vilche, J. R.; Ebert, M.; Juttner, K.; Lorenz, W. J. *J. Appl. Electrochem.* **1990**, *20*, 677.
(31) Pajkossy, T.; Nyikos, L. *Electrochim. Acta* **1989**, *34*, 171.
(32) Pajkossy, T. *Solid State Ionics* **1997**, *94*, 123.
(33) Kemer, Z.; Pajkossy, T. *J. Electroanal. Chem.* **1998**, *448*, 139.
(34) Vanmaekelbergha, D.; Ernébe, B. H. *J. Electrochem. Soc.* **1999**, *146*, 2488.
(35) Marsfeld, F.; Shi, H.; Greene, H.; Tsai, C. H. In *Electrochemical Impedance*: Scully, J., Silverman, D., Kending, M., Eds.; American Society for Testing and Materials: Philadelphia, PA, 1993.